Fermi National Accelerator Laboratory

FERMILAB-Conf-97/336-E
CDF

Jet Properties and QCD at High E_T

B. Flaugher
For the CDF Collaboration

Fermi National Accelerator Laboratory
P.O. Box 500, Batavia, Illinois 60510

October 1997

Published Proceedings of the *XVII International Conference on Physics in Collision*,
Bristol, UK, June 25-27, 1997

Operated by Universities Research Association Inc. under Contract No. DE-AC02-76CH03000 with the United States Department of Energy

JET PROPERTIES AND QCD AT HIGH E_T

B. FLAUGHER
Fermi National Accelerator Laboratory,
Batavia, IL 60510, USA

Results from the CDF and D0 collaborations on the inclusive jet, dijet and multijet cross sections are presented along with measurements of dijet angular distributions and multijet event variables.

1 Introduction

The Fermilab Tevatron provides the highest energy collisions ($\sqrt{s}$ =1.8 TeV) available in an accelerator, and is a unique place for testing QCD. Events with jets of $E_T > 400$ GeV have been identified in the CDF and D0 detectors. These high E_T jets probe the smallest distance scales, of $O(10^{-17})$ cm, and could provide the opportunity for observing new physics. High E_T measurements also provide information about the parton distribution functions and about the strong coupling constant α_s in kinematic regions not covered by other experiments.

Results discussed in this paper are based on the Run 1 data samples, roughly 110 pb^{-1} per experiment. Some results are presented separately for the Run 1A (15 pb^{-1} for D0 and 19.5 pb^{-1} for CDF) and Run 1B (roughly 90 pb^{-1} per experiment).

The data are compared to predictions from two NLO $O(\alpha_s^3)$ programs, EKS[1] and JETRAD[2], and two LO programs, HERWIG[3] and NJETS[4], where appropriate. Some of the theoretical uncertainties in these calculations will be discussed and quantified below.

2 Jet Identification

The detectors for CDF[5] and D0[6] have been described in detail elsewhere. The primary detector components used for these measurements are the calorimeters. For both experiments, detector response and jet energy corrections are derived from a combination of test-beam data and Monte Carlo simulations. In addition, CDF uses the central tracking chamber to provide in situ calibration of response to low P_T hadrons. Dijet balancing[7] is used by both experiments to determine the relative response of the large η calorimeters to the central calorimeter. Similarly, jet balancing in Z boson events is used as an in situ

calibration of the energy scale at D0 and as a check of the energy scale derived from the tracking information at CDF.

Jet clustering at the CDF and D0 experiments is performed using a cone algorithm where calorimeter cells within a radius $R \equiv (\Delta\eta^2 + \Delta\phi^2)^{1/2} = 0.7$ are grouped together to form a jet. Here $\eta \equiv -\ln[\tan(\theta/2)]$, where θ is the polar angle with respect to the beam line and ϕ is the azimuthal angle around the beam. The QCD calculations use a similar clustering algorithm. If two partons fall inside a cone they are merged into one "jet".

Both CDF and D0 measure the ambient energy in Minimum bias events and use this to represent the energy from fragmentation of partons not associated with the hard scattering. This underlying event energy is subtracted from the jets.

3 Inclusive Jet Cross Section: Experimental results

The inclusive jet cross section is a measurement of the number of events in a given bin of E_T normalized by the luminosity and acceptance. Last year CDF published [8] an inclusive jet measurement which showed an excess of events at high E_T. Figure 1 (left) shows the CDF data compared to EKS predictions using a renormalization scale of $\mu = E_T/2$, and MRSD0' parton distribution functions. The differences between MRSD0' and other PDF's are also shown. On the right, the CDF preliminary Run 1B measurement is shown compared to the Run 1A result. The two data sets are in good agreement and the excess above the theory is still present with the CTEQ3M PDF's. The systematic uncertainties on the CDF Run 1B data are expected to be roughly the same size as the Run 1A uncertainties.

In spring of 1997 D0 presented a new inclusive jet cross section measurement [9] which included a new jet energy scale and significantly reduced systematic uncertainties. This result in shown in Figure 2(left) compared to the prediction from JETRAD; good agreement with the theory is observed.

CDF and D0 have used different η ranges for these measurements (the D0 measurement covers $|\eta| < 0.5$ while the CDF measurement is for $0.1 \leq |\eta| \leq 0.7$) and made different choices for the theoretical parameters, with the result that it is difficult to directly compare the data using only Fig.s 1 and 2(left). In order to determine if the CDF and D0 data sets agree with each other, D0 has redone the inclusive jet analysis in the wider rapidity range (0.1-0.7) and fit the results to a smooth curve. This smooth curve is then compared to the CDF Run 1B data and is shown in Figure 2(right). The Run 1A CDF systematic uncertainties are shown along with the new preliminary D0 uncertainties. Over most of the E_T range the size of the uncertainties is equivalent. At high E_T the

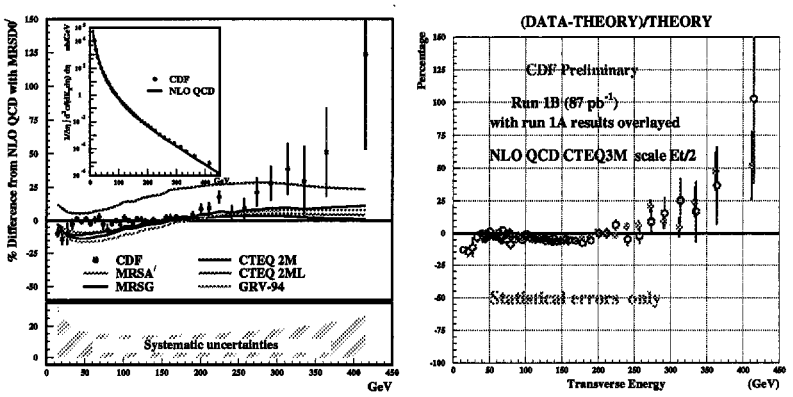

Figure 1: The published inclusive jet cross section as measured by CDF in the region $0.1 \leq |\eta| \leq 0.7$ compared to theoretical predictions from the EKS program with $\mu = E_T/2$ and various PDF's is shown on the left. The preliminary Run 1B measurement (right) is compared to the Run 1A result and to predictions using CTEQ3M PDF's.

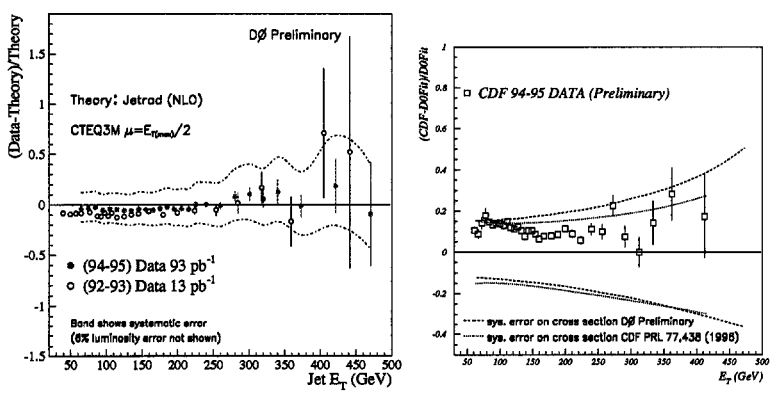

Figure 2: Inclusive Jet Cross section as measured by D0 and compared to theoretical predictions for $|\eta| < 0.5$ (left). On the right, a fit to a D0 measurement in the rapidity region $0.1 < |\eta| < 0.7$ is compared to the CDF Run 1B result. The systematic uncertainties shown are the Spring '97 D0 results. For CDF the Run 1A systematic uncertainties, which should be comparable in size to the Run 1B uncertainties, are shown.

CDF uncertainties are slightly smaller than those of D0. For this η region, the data sets seem consistent in shape and normalization within the experimental systematic uncertainties.

4 Inclusive Jet Cross Section: Theoretical uncertainties

Significant progress in understanding the theoretical uncertainties has been made since the publication of the CDF Run 1A results. For a recent summary, see for example Stirling this conference. In addition, detailed comparisons of EKS and JETRAD predictions have shown that the programs give the same results to better than 2% when the same input parameters (PDF's, μ scale etc.) are used [10]. Uncertainties from different parameter choices are discussed below.

4.1 Renormalization Scale μ

The EKS program performs an analytic calculation of the inclusive jet cross section at a given E_T and η. The convention of the EKS program is that the renormalization scale $\mu = CE_T^{jet}$, where C is a constant (usually in the range of 0.5 to 2.0). For the cross section at E_T^{jet}, this program integrates over all possible configurations in which a jet with E_T^{jet} appears. The PDF's and α_s are evaluated at this scale ($\mu = CE_T^{jet}$). The integration includes both two and three jet configurations. For example, in three jet events, the same configuration will appear at three different values of E_T^{jet}, and thus have a different contribution to the cross section at each E_T^{jet}. However, because the jet cross section is a steeply falling spectrum, the dominant contributions are those in which the highest E_T jet in the event is used to determine μ. For example, it is much easier to get an event with a 30 GeV jet and two 15 GeV jets than it is to get an event with a 60 GeV jet and two 30 GeV jets. With the EKS convention at a given E_T^{jet}, all the diagrams (leading order and next to leading order), α_s and the PDF's are calculated using same μ scale.

JETRAD is a Monte Carlo event generation program. The output of JETRAD is a 2 or 3 parton event and its corresponding weight. The choice of renormalization scale is taken to be the constant C (as defined above) times the transverse energy of the leading jet (E_T^{max}) or the ΣE_T of the jets in the event. The PDF's and α_s are evaluated at this value. With this convention a given bin of E_T^{jet} will have contributions from events in which different values of the μ scale were used.

Using a special version of the EKS code from D. Soper [11], the inclusive jet cross section using both, $\mu = E_t^{max}/2$ and $\mu = E_T^{jet}/2$ has been calculated.

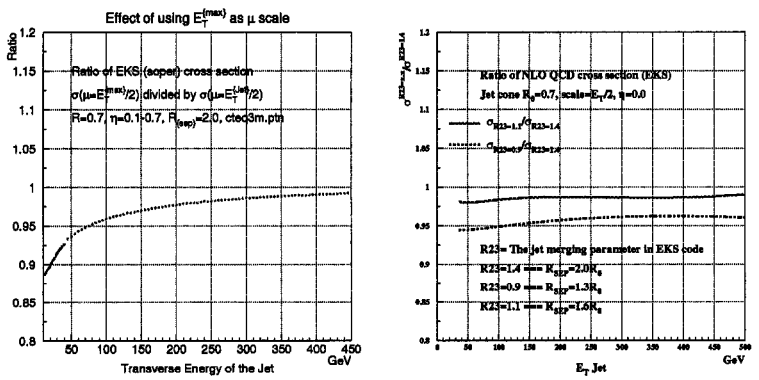

Figure 3: Left: comparison of NLO cross sections using $\mu = E_t^{max}/2$ and $\mu = E_T^{jet}/2$. The SOPER program is used, $R_{sep} = 2.0$, PDF's are CTEQ3M. Right: the variation of the inclusive jet cross section for different R_{sep} parameters.

Figure 3 shows the ratio of the cross sections calculated with μ=$E_T/2$ and μ=$E_T^{max}/2$. The effect of using μ=$E_T^{max}/2$ instead of μ=$E_T/2$ ranges from $\approx$ 4% at 100 GeV to < 1% at 450 GeV. The difference increases with decreasing E_T because a larger fraction (but still small) of the jets are the second or third jet in the event. As the μ scale used in the $\mu = E_T^{jet}$ convention is less than or equal to the maximum E_T jet in an event, the cross section for the $\mu = E_T^{Jet}$ case is slightly larger (α_s is larger).

4.2 Cluster/parton merging

An additional parameter, R_{sep}, has been introduced to the NLO calculations to mimic the effects of cluster merging in the data. Rather than requiring that two partons be 2R apart to form separate jets, an R_{sep} of 1.3 requires a separation of 1.3R to form separate jets. CDF typically has used R_{sep} =2.0 while D0 has chosen R_{sep} =1.3 for the theoretical predictions [12]. The ratio of QCD predictions using R_{sep} = 1.3 and R_{sep} = 2 is shown Fig.3. As expected the cross section is smaller with the smaller R_{sep} because of the smaller effective cone size. There is a 5% change in the cross section which is almost independent of jet E_T. This result is consistent with previous results [13] where the comparison uses $\mu = E_T/4$ and different parton distribution functions.

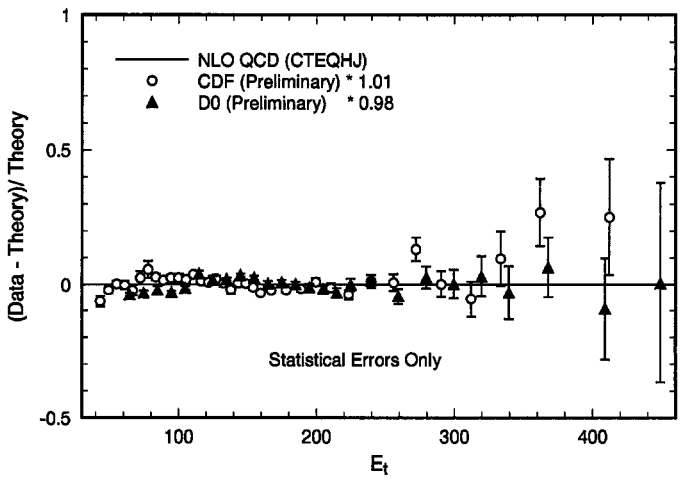

Figure 4: Inclusive Jet Cross sections measured by CDF and D0 compared to QCD predictions using the CTEQ4HJ PDF's (which included the CDF and D0 data in the global fit).

4.3 Parton Distribution Functions

By far, the largest uncertainty in the inclusive jet cross section predictions comes from the uncertainty in the parton distribution functions. Recent estimates of the size of this uncertainty come from exercises performed by the CTEQ and MRS collaborations where they included the CDF and D0 data in the global PDF fitting packages [14]. Figure 4 shows the CDF and D0 data compared to NLO QCD with the resulting PDF, CTEQ4HJ. Reasonable agreement is observed in the high E_T region showing that it is possible to fit this data within the framework of standard QCD.

More data is clearly needed to constrain the predictions. Data from the direct photon fixed target experiment E706 at Fermilab should provide some information about the gluon distribution. In addition, jet cross section measurements at high η (described below) can be used to probe high x while the jet E_T remains in the region of good agreement with QCD.

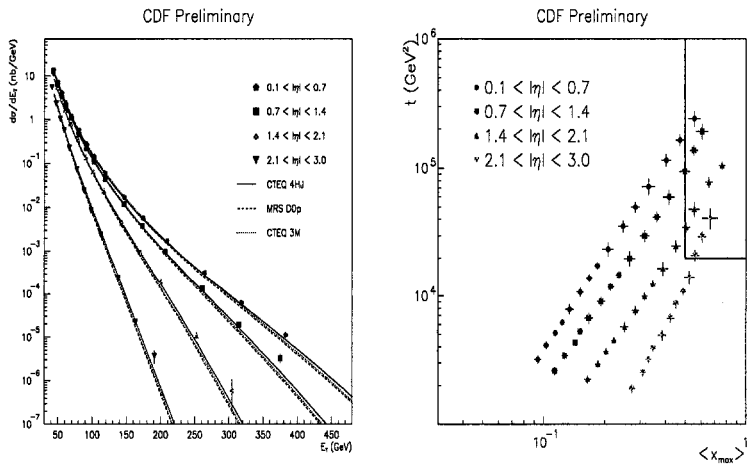

Figure 5: Left: Comparison of data and NLO cross sections in the different rapidity bins. Right: CDF dijet differential cross sections plotted in terms of x and Q^2. Only statistical uncertainties are shown.

5 Di-jet Measurements

5.1 Inclusive Di-jet Differential Cross Section

Measurements of the dijet differential cross sections in different rapidity regions can provide additional information and constraints on the QCD predictions. By restricting the E_T and rapidity of the jets in the events, different regions of x and Q^2 can be probed. In the CDF measurement, the two highest E_T jets are identified and one is required to be in the central ($0.1 \leq |\eta| \leq 0.7$) region. Because the central region has the smallest energy scale uncertainty, the central jet is used to measure the E_T of the event. The other jet, called the "probe" jet, is required to have $E_T > 10$ GeV and to fall in one of the η bins: $0.1 \leq |\eta| \leq 0.7$, $0.7 \leq |\eta| \leq 1.4$, $1.4 \leq |\eta| \leq 2.1$, $2.1 \leq |\eta| \leq 3.0$. There are no restrictions on the presence of additional jets. Figure 5(left) shows the cross section in the individual η bins as a function of the central jet E_T. JETRAD is used for the theoretical predictions with renormalization scale $\mu = E_T^{max}/2$. The data are compared to the predictions using three parton distribution functions, CTEQ4HJ, MRSD0' and CTEQ3M. The statistical uncertainty is shown on the points; the systematic uncertainty is under study.

The different rapidity bins correspond to different regions of x and Q^2. At leading order the parton momentum fraction x is related to the E_T and η of

the jets by the equations:

$$x_1 = \frac{E_T}{\sqrt{s}}(e^{\eta_1} + e^{\eta_2}), \quad x_2 = \frac{E_T}{\sqrt{s}}(e^{-\eta_1} + e^{-\eta_2})$$

but at large η and E_T many (25-60%) of the events have more than 3 jets with E_T >10 GeV. To account for at least one additional jet the following equations are used:

$$x_1 = \frac{E_{T1}}{\sqrt{s}}(e^{\eta_1} + \frac{E_{T2}}{E_{T1}}e^{\eta_2} + \frac{E_{T3}}{E_{T1}}e^{\eta_3})$$

$$x_2 = \frac{E_{T1}}{\sqrt{s}}(e^{-\eta_1} + \frac{E_{T2}}{E_{T1}}e^{-\eta_2} + \frac{E_{T3}}{E_{T1}}e^{-\eta_3}).$$

For each bin of E_T the average value for the factor in the brackets is calculated and multiplied by the corrected E_{T1} to determine x. The factors have been ordered so that x_1 is always the maximum. For a two body process,

$$Q^2 \sim -\hat{t} = \frac{\hat{s}}{2}(1 - \cos\theta^*) = 2E_T^2 \cosh^2 \eta^*(1 - \tanh \eta^*).$$

Figure 5(right) shows the CDF data for each bin plotted in terms of x and Q^2. The data is seen to overlap with the high x and Q^2 region which has been of interest at HERA. The error bars represent only the statistical uncertainty.

5.2 Di-jet mass spectrum

D0 and CDF have both measured the dijet mass spectrum. D0 has performed this measurement in two rapidity regions: central, $|\eta| < 0.5$, and more forward, $|\eta| < 1.0$, $|\Delta\eta| < 1.6$. The dijet mass at D0 is defined assuming massless jets: $M_{jj} = \sqrt{2E_T^1 E_T^2(cosh(\Delta\eta) - cos(\Delta\phi))}$. Figure 6 shows the D0 data compared to predictions from JETRAD for both rapidity regions. The systematic uncertainties are also shown. Note that these results have the previous (1996) jet energy scale corrections. Figure 6 shows the difference between data and theoretical predictions on a linear scale. The data agrees with the predictions within the systematic uncertainties.

The CDF measurement of the dijet mass uses the four-vector definition for the mass: $M_{jj} = \sqrt{(E_1 + E_2)^2 - (\mathbf{P_1} + \mathbf{P_2})^2}$ and a larger rapidity region than the D0 measurement, $|\eta| < 2.0$. To ensure good acceptance, CDF also imposes a cut on $|cos\theta^*| < 2/3$, where θ^* is the dijet scattering angle in the center-of-mass frame. Figure 7 shows the CDF data compared the the JETRAD predictions. The shaded band shows the preliminary estimate of the systematic uncertainties. Different PDF's are shown. CTEQHJ seems to provide the best agreement with the data in the high E_T region.

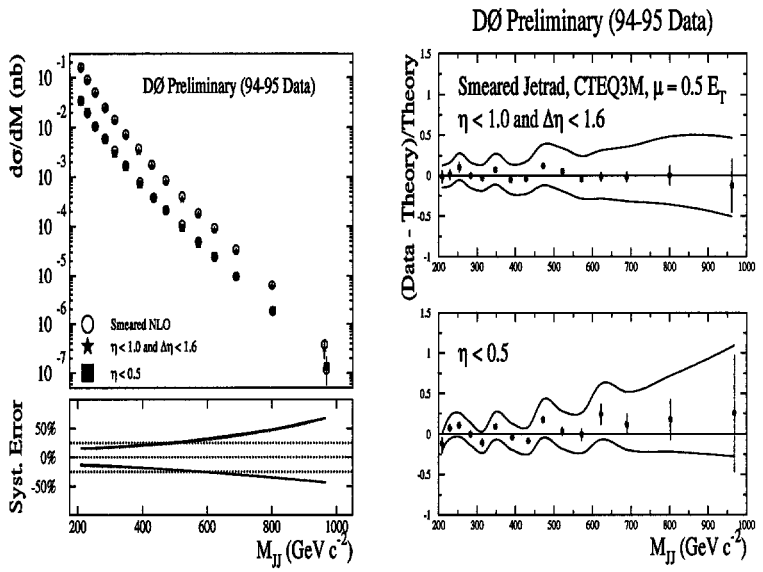

Figure 6: Dijet mass as measured by D0 for two rapidity ranges and compared to NLO QCD predictions.

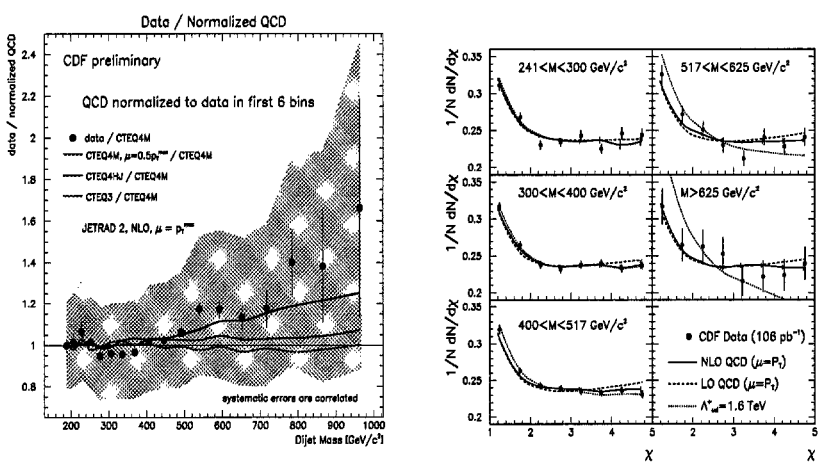

Figure 7: Left: difference between dijet mass spectrum as measured by CDF and NLO QCD predictions. Right: Dijet angular distribution as measured by CDF for different mass ranges compared to LO and NLO QCD predictions.

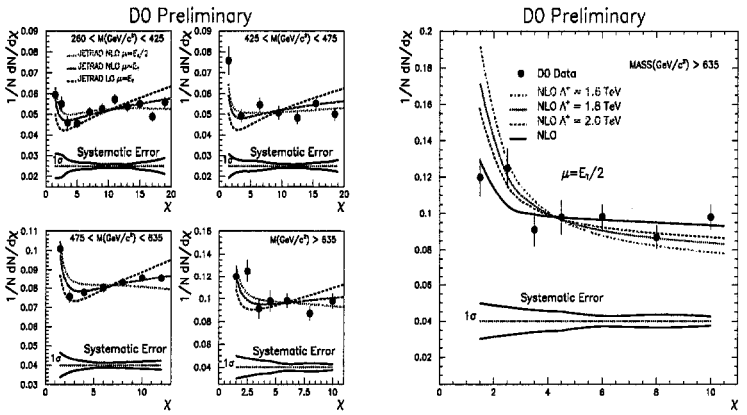

Figure 8: Dijet angular distribution as measured by D0 for different mass ranges compared to LO and NLO QCD predictions (left) and compared to predictions with additional contributions from composite quarks (right).

5.3 Di-jet angular distributions

CDF and D0 have both completed analyses of the di-jet angular distribution[15]. The dijet angular distribution is unique among these high E_T measurements in that it is almost independent of the parton distribution functions. The shape of the angular distribution is dominated by t-channel exchange, and is nearly identical for all the dominant subprocesses. This provides an independent way to look for the effect of new physics. Both experiments use the variable $\chi = \frac{1+|cos\theta^*|}{1-|cos\theta^*|}$ for this measurement. Most new physics models predict an isotropic angular distribution which would produce a peaking at low χ. Limits on compositeness are derived from the ratio of the number of events at low χ to those in the high χ region.

Figure 7 shows the CDF data compared to QCD predictions (JETRAD) for different mass bins. In the highest mass bin the prediction for QCD plus compositeness is shown. To set compositeness limits CDF and D0 both use the NLO JETRAD prediction times a "k-factor" from LO QCD + compositeness. NLO calculations with compositeness are not available. The CDF compositeness limits are based on the ratio of number of events below and above χ= 2.5. The data exclude at the 95% C.L. a contact interaction scale of $\Lambda^+_{ud} \leq 1.6$ TeV and $\Lambda^-_{ud} \leq 1.4$ TeV. For a model where all quarks are composite $\Lambda^+ \leq 1.8$ TeV and $\Lambda^- \leq 1.6$ TeV.

The D0 measurements cover a larger region in χ and are shown in Figure 8. The NLO predictions from JETRAD with $\mu = E_T$ provides the best agreement with the shape of the data. The limits in this analysis are derived from the ratio of the number of events above and below χ=4. The D0 data excludes (at the 95% CL) contact interaction scales with $\mu = E_{Tmax}$: $\Lambda^-_{ud} \leq 2.0$ TeV, $\Lambda^- \leq 2.2$ TeV, $\Lambda^+ \leq 2.1$ TeV, and with $\mu = E_{Tmax}/2$: $\Lambda^-_{ud} \leq 2.2$ TeV, $\Lambda^- \leq 2.4$ TeV, $\Lambda^+ \leq 2.3$ TeV.

6 Multijet Physics

Studies of multijet events provide additional probes of high E_T events. In these events, the total E_T ($= \Sigma E_T^{jet}$), is large but it is often distributed over many jets. For a multijet system, many kinematic variables are needed to describe the system and can be compared to theoretical predictions. CDF and D0 have performed analyses which look at many of these variables[16]. In addition CDF has measured the total cross section as a function of the ΣE_T^{jet} in the events[17].

6.1 Multijet variables

In its rest frame an N-Jet system can be defined by 4N-4 independent variables. For a 3-jet event these 8 variables are:

- m_{3j}
- Dalitz variables x_3, x_4: $x_j = \frac{2E_T}{m_{3j}}$ where final state jets are ordered $E_3 > E_4 > E_5$
- $\cos\theta_3$, where θ_3 = leading jet scattering angle
- Ψ_3, the angle between 3-jet plane and the plane containing the leading jet and the beam
- jet mass variables: $f_j = \frac{m_j}{m_{3j}}$

For a 4-jet event, the system is reduced to 3 bodies by combining the two jets with lowest two-body mass. This results in m_{4j} + 7 three-jet variables + 4 variables defining how the two jets are combined, for a total of 12 variables.

The 5-jet events are treated in a similar manner: 5 bodies are reduced to 4 bodies and then to 3 bodies for a total of 16 variables. Similarly, for 6-jet events, resulting in a total of 20 independent variables. The data contains 3, 4, 5 and 6 jet events, giving a grand total of 56 variables which can be compared to the theoretical predictions.

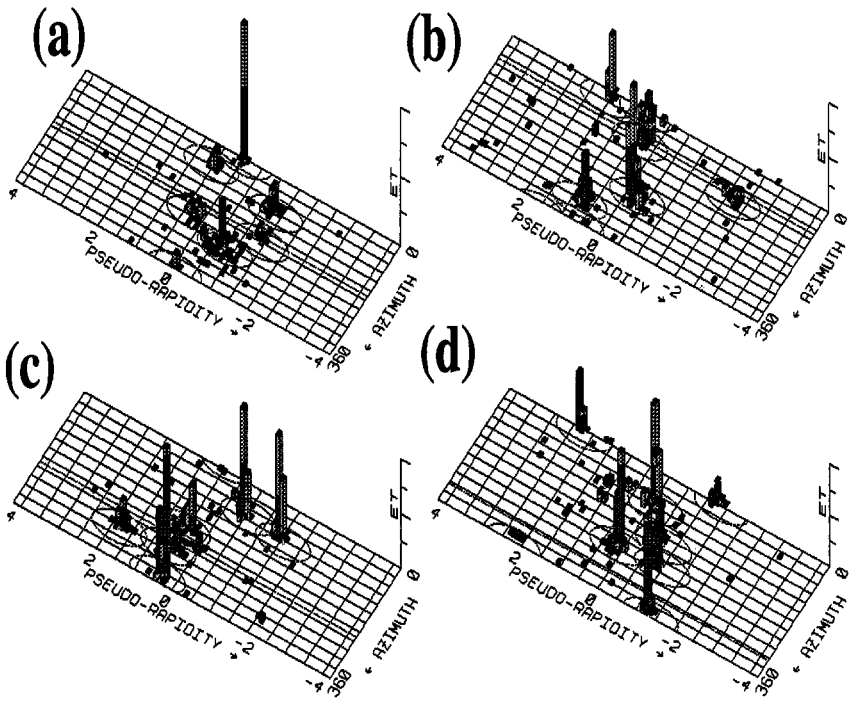

Figure 9: Four 6-jet events in the CDF detector.

The event samples for the multijet analysis are defined by cuts which ensure good acceptance. The inclusive multijet samples are determined after jet corrections and background removal. The minimum jet E_T used in this analysis is 20 GeV, x_3 <0.9 and cos θ_3 <0.6.

For events with $\geq$ 3-jets, additional requirements of $\Sigma E_T > 420$ GeV and $m_{3j} > 600$ GeV/c^2 are imposed to avoid bias from the trigger. These cuts result in 1021 events; of these 320 have $\geq$ 4 jets. For events with $\geq$ 6-jets the additional requirements are $\Sigma E_T > 320$ GeV and $m_{6j} > 520$ GeV/c^2. This results in 1282 events, 26 of which have $\geq$ 7 jets. Figure 9 shows four 6-jet events in the CDF detector.

The data are compared to QCD predictions from HERWIG and NJETS plus detector simulations. HERWIG is a shower Monte Carlo which uses $2 \rightarrow 2$ matrix elements. These calculations use CTEQ2L for the PDF's. The NJETS program uses QCD $2 \rightarrow N$ matrix elements, for N=2,...5 and for N=6 an approximation is used. Min. parton separation for these analysis is 0.9 and the PDF's are CTEQ3L. The data are also compared to a Phase Space Model where the $m_N j$ and $\frac{m_j}{m_{Nj}}$ distributions have been matched to those from HERWIG.

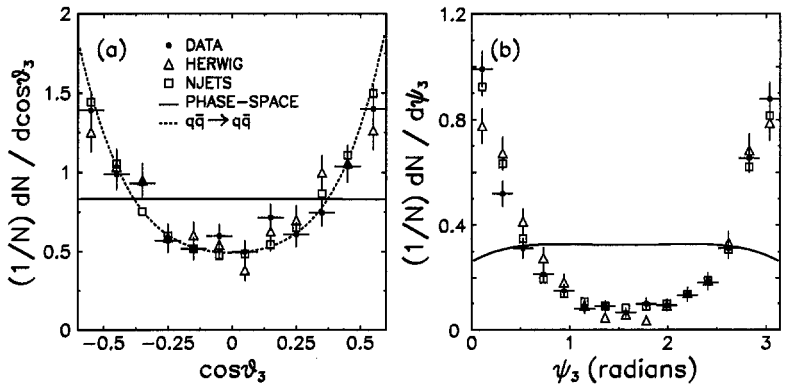

Figure 10: Distributions of $cos\theta^*$ and ψ for events with $\geq$ 3 jets as measured by CDF compared to theoretical predictions.

Both HERWIG and NJETS give reasonable descriptions of all 56 variables. Figures 10 and 11 show the $\cos\theta_3$ and the Ψ_3 distributions for the events with $\geq$ 3 jets and for events with $\geq$ 6 jets. Good agreement between the data and QCD predictions is observed while the data is clearly in disagreement with the phase space model.

6.2 Differential Cross Section for Multijet Events

CDF and D0 both measure the cross section for multijet events as a function of the total transverse energy ΣE_T^{jet}, where the sum is over all jets passing a given E_T threshold. At CDF two jet thresholds are used, 20 GeV and 100 GeV, to separate soft and hard contributions to the cross section. A threshold of $\Sigma E_T^{jet} > 320$ GeV within $\eta < 3.5$ and is used for the CDF analysis resulting in 141,041 events with the 20 GeV threshold and 71,611 events for the 100 GeV threshold. For this analysis the data are compared to predictions from HERWIG with CTEQ2L PDF's and renormalization scale $Q^2 = stu/2(s^2+u^2+t^2)$ and to predictions from JETRAD with CTEQ4M PDF's, and renormalization scale $= 0.5\Sigma E_T^{jet}$.

Figure 12 shows the CDF data compared the predictions for the 20 and 100 GeV thresholds. Note that the normalization for the 20 GeV measurement is not well predicted by LO or NLO QCD, while there is much better agreement with NLO QCD for the 100 GeV threshold. LO QCD predictions from HERWIG are expected to have a large uncertainty in normalization from the choice of scale and thus it is not surprising that the overall normalization is not

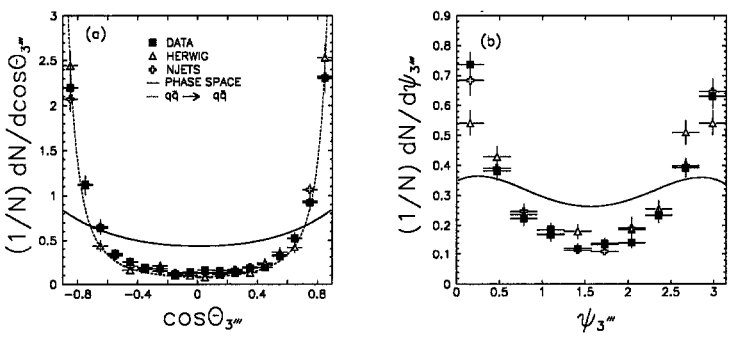

Figure 11: Distributions of $cos\theta^*$ and ψ for events with $\geq$ 6 jets as measured by CDF compared to theoretical predictions.

in good agreement with the data. JETRAD is a NLO $2 \rightarrow 2$ calculation which can have 2 or 3 jets in the final state. However, in the data, with E_T >20 GeV, 31% of the events have >3 jets. For a 100 GeV jet E_T cut 95% have only 2 jets. This suggests that the effects of higher order terms are reduced by a high jet threshold. Sensitivity to renormalization scale is also an indication of the influence of higher order terms. Changing the μ scale from $\Sigma E_T/2$ to $\Sigma E_T/4$ increases the predicted NLO cross section by 26% for the 20 GeV cut and only 7% for the 100 GeV cut. Thus, there are clearly contributions from higher order terms in the multijet sample from the high multiplicity of jets in the events. These effects can be minimized, both in the data and in the theory, through the use of a high jet threshold.

DO has used the measurement of the ΣE_T cross section as a test for new physics. Figure 13 shows the D0 data compared to QCD predictions. The variable $H_T = \Sigma E_T^{jet}$, where the jet threshold used is 20 GeV and the data is normalized to the predictions at 500 GeV. The predictions are from JETRAD with renormalization scale $\mu = E_T^{max}/2$ and CTEQ3M PDF's. A new physics signal would show up as an enhancement of the cross section at high H_T. The data is consistent with the QCD predictions within the systematic uncertainty and a limit on compositeness will soon be derived.

7 Conclusions

CDF and D0 have both measured the inclusive jet cross section and compared their data to theoretical predictions. For the rapidity region $|\eta|$ <0.5 D0 sees

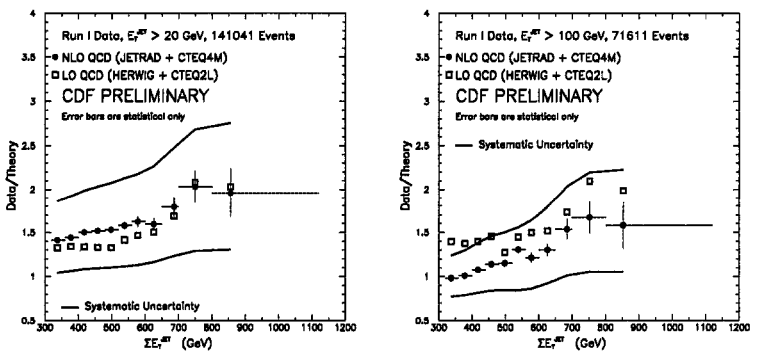

Figure 12: CDF multijet differential cross section for jet thresholds of 20 GeV (left) and 100 GeV (right) compared to theoretical predictions.

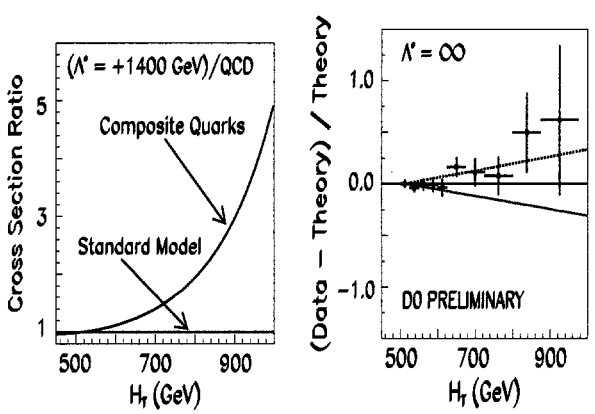

Figure 13: D0 multijet differential cross section and systematic uncertainty compared to QCD predictions.

good agreement with NLO QCD. In the rapidity region $0.1 < |\eta| < 0.7$, the CDF data shows an excess over the theoretical predictions. A direct comparison in the rapidity region $0.1 < |\eta| < 0.7$ shows that the CDF and D0 data are in agreement within the experimental uncertainties. Since the publication of the CDF Run 1A results, there has been much progress in understanding theoretical uncertainties. In particular, the flexibility of the PDF's is large and not fully constrained by data.

Measurement of the differential dijet cross sections at large η allows exploration of the high x and Q^2 region and may be useful in constraining the parton distribution functions. Preliminary results from CDF show good agreement with NLO QCD at low E_T. Preliminary results from CDF and D0 on the dijet mass spectra show agreement with NLO QCD predictions within the preliminary systematic uncertainties. Results on the dijet angular distributions at CDF and D0 are essentially final and agree with NLO QCD. The best limits on compositeness are now from D0: $\Lambda^+ \geq 2.1$ TeV, $\Lambda^- \geq 2.2$ TeV.

The study of multijet events shows that both the shower Monte-Carlo HERWIG and the N-JETS matrix element program are in good agreement with the data. JETRAD gives reasonable agreement with data for the multijet differential cross section. By studying the sensitivity to jet threshold and renormalization scales, CDF has shown that a high jet threshold reduces the sensitivity to higher order terms. D0 has also used the cross section as a test for new physics.

In summary, the Tevatron measurements of high E_T jet phenomena continue to challenge the limits of the theoretical predictions.

References

1. S. Ellis. Z. Kunszt, and D. Soper, Phys. Rev. Lett. **62** 2188 (1989), Phys. Rev. Lett. **64** 2121 (1990) Phys. Rev. D **40** 2188 (1989).
2. W. T. Giele, E.W.N. Glover and D.A. Kosower, Nucl. Phys. **B403** 633 (1993).
3. G. Marchesini and B. Webber,Nucl. Phys. **B310**, 461 (1988).
4. F.A. Berends, and H. Kuijf, Nucl. Phys. **B353**, 59 (1991).
5. CDF Collaboration, F. Abe et al., Nucl.Instrum.Meth. A271 (1988) 387
6. D0 Collaboration, S. Abachi et al., Nucl. Instrum, and Methods, A **338**, 185 (1994).
7. CDF Collaboration, F. Abe et al., Phys. Rev. D **47** 4857 (1993). D0 Collaboration, S. Abachi et al., Phys. Lett. B **357**500 (1995). D0 Collaboration, R.Kehoe, Proc. 6th International Conf. on Calorimetry in High Energy Physics, Frascati (1996), Fermilab-Conf-96/284-E.

8. CDF Collaboration, F. Abe et al., Phys. Rev Lett. **77** 438 (1996).
9. F. Nang (CDF and D0 collaborations), Proc. of 32nd Rencontres de Moriond: QCD and High-Energy Hadronic Interactions, Les Arcs, France, 22-29 Mar (1997). FERMILAB-CONF-97-192-E.
10. A. Bhatti and B. Flaugher, "Uncertainties in the NLO QCD predictions for Inclusive Jet Cross Section" CDFnote 4014.
11. Z. Kunszt, and D. Soper, Phys. Rev. D **46** 192(1992), and http://zebu.uoregon.edu/ soper/soper.html, program version 3.4.
12. D0 Collaboration, B. Abbott et al., FERMILAB-PUB-97-237-E.
13. S. Ellis Proc. of 28th Rencontres de Moriond: QCD and High Energy Hadronic Interactions, Les Arcs, France, 20-27 Mar (1993) Hadronic: 235-244; hep-ph/9306280.
14. H.L. Lai et al, Phys. Rev. D **55** 1280 (1997) and A.D.Martin, R.G.Roberts, W.J.Stirling, Phys. Lett. B387 419 (1996).
15. CDF Collaboration, F. Abe et al., Phys. Rev. Lett. **77** 5336 (1996). D0 Collaboration, B. Abbott et al., FERMILAB-PUB-97-237-E.
16. CDF Collaboration, F. Abe et al., Phys. Rev. D **54** 4221 (1996) and **56** 2532 (1997). D0 Collaboration, B. Abbott et al., Phys.Rev. D53, 6000 (1996).
17. CDF Collaboration, F. Abe et al., FERMILAB-PUB-97-290-E.